RESEARCH PAPER

Tailoring Microstructure and Mechanical Properties of Nano/Ultrafine Grained AA6063 Alloy Processed by Accumulative Roll Bonding Process

H. R. Jafarian[1,2,*] and H. Miyamoto [3]

** jafarian@iust.ac.ir*

Received: June 2019 Revised: September 2019 Accepted: January 2020

[1] School of Metallurgy and Materials Engineering, Iran University of Science and Technology, Tehran, Iran.

[2] Center for International Scientific Studies and Collaboration, Ministry of Science, Research and Technology, Tehran, Iran.

[3] Department of Mechanical Engineering, Doshisha University, Kyotanabe, Kyoto, Japan.

DOI: 10.22068/ijmse.17.1.1

Abstract: *In the present work, accumulative roll bonding (ARB) was used as an effective method for the process of nano/ultrafine-grained AA6063 alloy. Microstructural characteristics indicate considerable grain refinement leading to an average grain size of less than 200 nm after 7 ARB cycles. Texture analysis showed that 1-cycle ARB formed a strong texture near the copper component ({112}<111>). However, texture transition appeared by increasing the number of ARB cycles and after the 7-cycle of ARB, the texture was mainly developed close to the rotated cube component ({100}<110>). The results originated from mechanical properties indicated a substantial increment in strength and microhardness besides a meaningful drop of ductility after the 7 ARB cycles.*

Keywords: *Aluminum AA6063, Accumulative roll bonding, Nano/Ultrafine grained microstructure, Texture characterization, Mechanical properties.*

1. INTRODUCTION

Improving the mechanical strength of metallic materials without degradation of their ductility and formability properties is of high demands due to their wide application in all engineering sectors. It is well known that manipulating the microstructure via grain refinement down to ultrafine or nanoscale is an excellent method to enhance the mechanical properties in order to enable more effective exploitation of the metallic materials [1–3]. Severe plastic deformation (SPD) is an extensively strengthening method because it involves an effective refinement for microstructure engineering in metallic materials down to ultrafine or nanoscale regimes [4–6].

Recently, accumulative roll bonding (ARB) has been demonstrated as a capable technique in generating ultrafine/nanostructured materials in the form of particulate metal matrix composites (MMCs) and bimetallic or tri-metallic composites [7–9]. In the ARB process, in the first step 2 pieces of metallic sheets with identical length, width and thickness are prepared, stacked and roll bonded with a rolling machine. In the next step, the bonded sheet is cut into two identical splits, and then the specimens are wire brushed and stacked together for the second ARB cycle. During recent decades, the ARB has attracted many researchers' attention because of the numerous unique features of this approach compared to other SPD methods or conventional rolling [2,3,10–18]. As a result, there have been numerous studies of this method and a mature level of understanding of the mentioned methods used and the microstructural development that occurs during the ARB. Also, it was shown that the ARB is a promising technique to improve material strength. However, low uniform ductility is generally exhibited by the SPD processed materials [11,19,20]. Recently, producing ultrafine-grained composite sheets by employing soft and hard materials has been found to be a solution to this problem [8].

The AA6063 alloy has been widely used in industry due to good weldability, good formability, high levels of corrosion resistance, and good superplasticity [21–23]. Accordingly, the objective of the present paper focused on texture development and mechanical properties with respect to microstructure evolution in an AA6063 alloy processed by the accumulative roll bonding process.

[DOI: 10.22068/ijmse.17.1.1]

2. EXPERIMENTAL PROCEDURE

In this study, AA6063 alloy with the composition shown in table 1 was cut into 150 mm × 50 mm × 1 mm and these were annealed at 673 K for 2 h. The ARB processing diagram is illustrated in Fig. 1. After surface preparation (degreasing in acetone and wire-brushing with a stainless-steel brush), the two sheets were stacked and tied with copper wire at both ends to ensure that the strips don't slide during the rolling process. Finally, the fourth step is rolling with a 50% reduction without any lubricant at ambient temperature. The roll diameter was 310 mm and the roll peripheral speed was about 13 rpm. This procedure was repeated for up to 7 cycles.

Microstructural characterization was performed using a field-emission type scanning electron microscope (SEM/Philips XL30S-FEG) equipped with an electron backscatter diffraction (EBSD) detector. TSL-OIM analysis software was used to analyze the EBSD data. The texture was evaluated by measuring incomplete pole figures (PFs) of {111}. Orientation distribution functions (ODFs) were calculated using Bunge's series expansion method, with an expansion degree of lmax = 22 in Euler space.

The strip tensile test specimens were machined according to the ISO 6892–01 standard tensile sample. The gauge width and length of the tensile samples were 5 ± 0.1 mm and 10 ± 0.1 mm, respectively. The test was performed using a Hounsfield H50KS tensile testing machine at an initial strain rate of 10-3 s-1. Moreover, the total elongation of each specimen was measured by the difference in the gauge length before and after testing.

Microhardness was measured on the plane of rolling direction-transverse direction (RD-TD) under a load of 200 g for 20 s. Also, deformation inhomogeneity was quantitatively evaluated as inhomogeneity factor (IF) using the following expression [22]:

Table 1. Chemical composition of the AA6063 alloy used in this study.

Element (wt. %)	Al	Mg	Si	Fe	Zn	Cu	Ti	Mn	Cr
AA6063	Balance	0.85	0.46	0.32	0.13	0.06	0.05	0.04	0.04

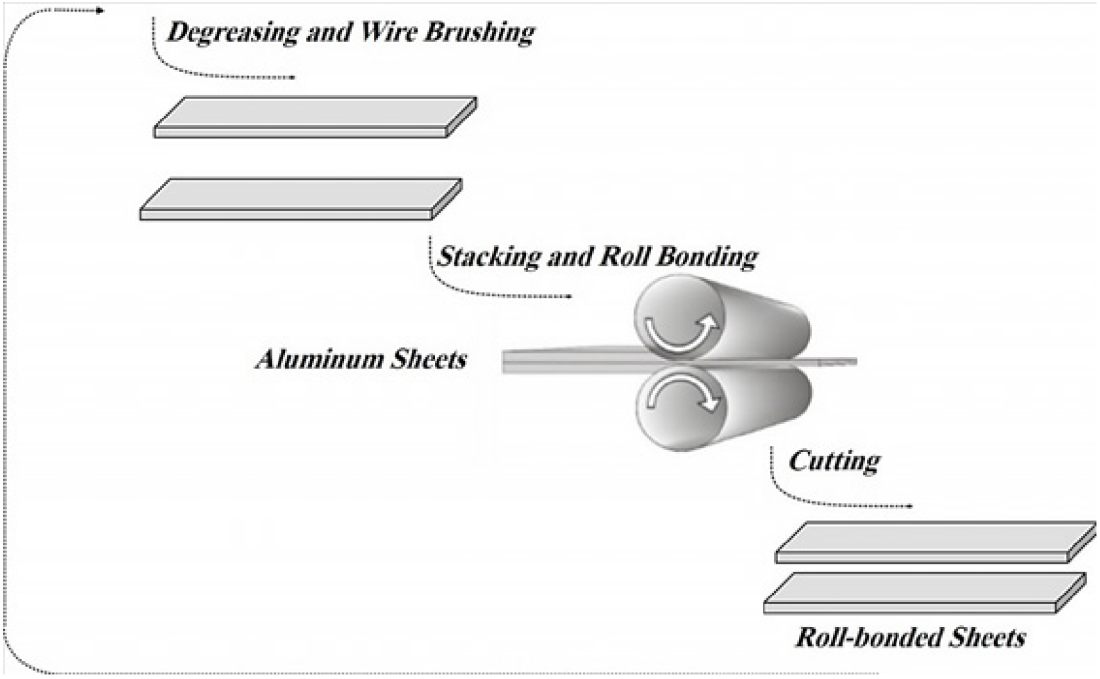

Fig. 1. Schematic of accumulative roll bonding processing.

[DOI: 10.22068/ijmse.17.1.1]

$$IF = \frac{\sqrt{\sum_{i=1}^{n}\left(HV_i - HV_{ave}\right)^2/(n-1)}}{HV_{ave}} \times 100 \qquad (1)$$

where n , HV_i , and HV_{ave} are the number of microhardness measurements for each sample, the microhardness value of i^{th} measurement and the average microhardness value, respectively.

3. RESULTS AND DISCUSSION

3.1. Microstructure Characterization

Fig. 2 shows the starting microstructure in the state of as-received strip subjected to full annealing at 673 K for 2 h. The figure indicated that the average grain size is about 45 µm and the starting material exhibits fully equiaxed grains.

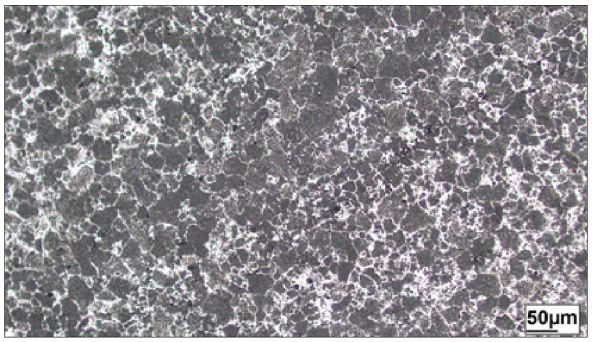

Fig. 2. Microstructure of the annealed AA6063 specimen before the accumulative roll bonding process.

Inverse pole figure EBSD orientation color map and grain boundary map from the RD-ND planes obtained by EBSD measurements together with their analyses for the 1-cycle, 3-cycle, and 7-cycle ARB processed specimens are illustrated in Fig. 3. In the grain boundary maps, high angle grain boundaries (HAGBs) having misorientation larger than 15° and low angle grain boundaries (LAGBs) having misorientation between 2° and 15° are displayed by black and red lines, respectively. To prevent any inaccuracy during measurement by the EBSD, the boundaries having misorientation less than 2° are not considered. The grain boundary map of the 1-cycle ARB specimen is essentially a normal deformation microstructure consisting of pancake shape grains having a large volume fraction of low angle boundaries (Fig. 3(a)). By reaching a 3-ARB cycle, the fraction of low angle boundaries decreases and the fraction of high angle boundaries increases as shown in Fig. 3(b). Likewise, a non-uniform grain size distribution is observed. After seven ARB cycles (Fig. 3(c)), the entire sample is covered by semi equiaxed alongside elongated grains in the rage of ultrafine-grained regions. The average grain size is about 200 nm and the distribution of grain size is almost uniform. It is well clarified that the formation mechanism of nano/ultrafine grains in severely deformed metals consisted of three sequential stages, i.e., the appearance of dislocation cells or formation of subgrain structure, the transformation of LAGBs to HAGBs and eventually migration of new HAGBs [24–27]. Also, the severe shear strain resulted from friction between the strips and the rolling during the ARB can be considered as another important reason for grain refinement [28].

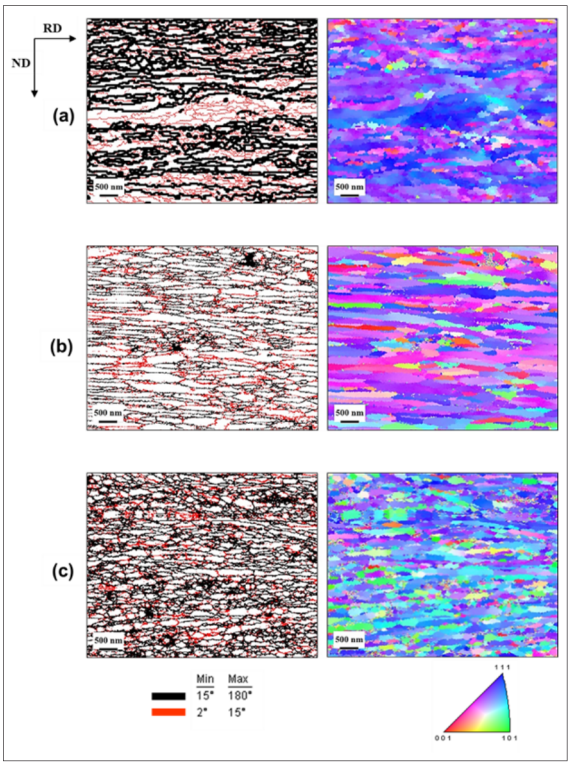

Fig. 3. Inverse pole figure EBSD orientation color map and grain boundary map of ARB processed AA6063 after (a) 1, (b) 3 and (c) 7 cycles.

3.2. Texture Characterization

Fig. 4 shows {111} pole figures obtained from EBSD data and analysis of the starting material, 1-cycle, 3-cycle, and 7-cycle ARB processed spec-

[DOI: 10.22068/ijmse.17.1.1]

imens, respectively. The positions of ideal orientation for typical texture components for FCC crystal, i.e., brass orientation ({110}<112>), copper orientation ({112}<111>), S orientation ({123}<634>), rotated cube orientation ({100}<110>), Dillamore orientation ({4 4 11}<11 11 8>) and Goss orientation ({110}<001>), are also plotted in the pole figures of Fig. 4. The results of pole figures proved that the starting material clearly demonstrates not any kind of texture, i.e., it means that it has a random texture as shown in Fig. 4 (a). This could be a characteristic of the recrystallized state [29–31]. In contrast, the results obtained from pole figures of the ARB processed specimens indicate that almost all of them are symmetric and they demonstrate a kind of dominant orientation or texture. Fig. 4 (b) indicates that 1-cycle ARB develops the copper component ({112}<111>) as the main texture alongside Dillamore component ({4 4 11}<11 11 8>). Increasing the level of strain through ARB brings about the texture transition, and the results proved that the preferred orientation develops mainly around rotated cube orientation ({100}<110>) by the 3-cycle of ARB together with copper orientation ({112}<111>) as seen in Fig. 4 (c). Eventually, Fig. 4 (d) exhibits the {111} pole figure of the 7-cycle ARB processed specimen representing a strong texture close to the rotated cube ({100}<110>) and Goss orientations ({110}<001>).

The texture evolution of the ARB processed specimens indicated that all the pole figures with different ARB cycles were symmetric. The texture of the 1-cycle ARB processed specimen exhibits very strong texture close to the copper component ({112}<111>) as the main texture, and to some extent, Dillamore orientation ({4 4 11}<11 11 8>)

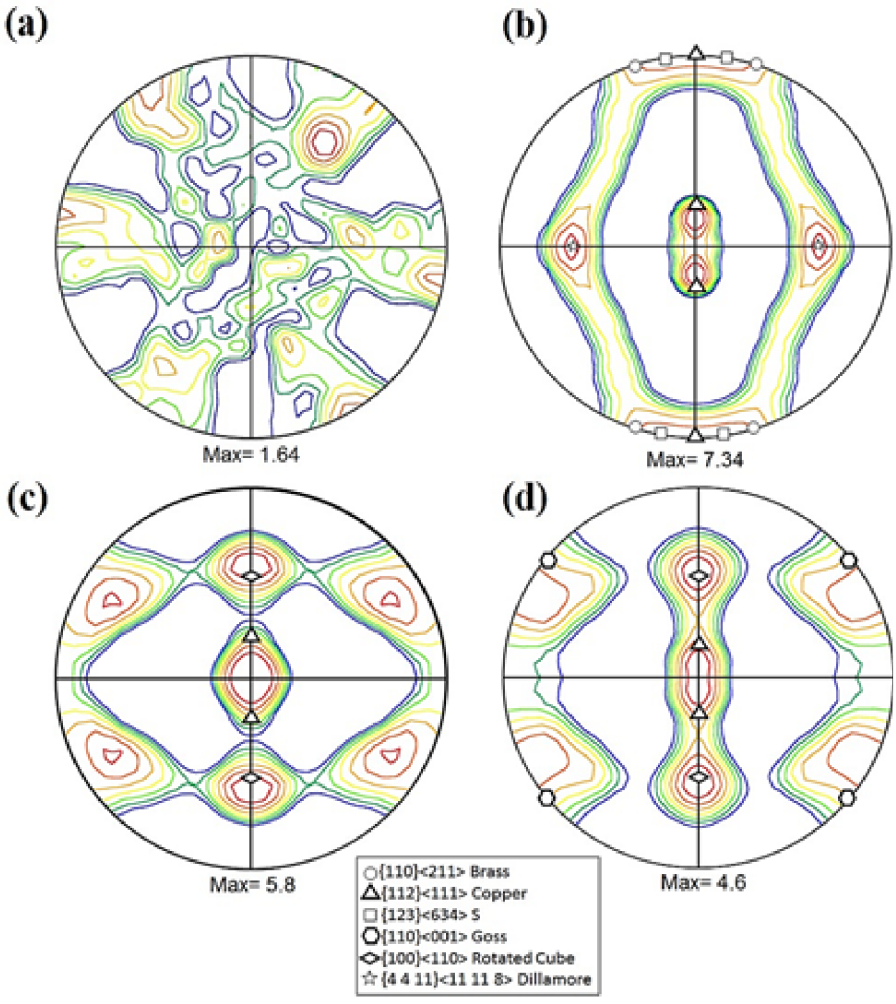

Fig. 4. {111} pole figures of (a) the starting material, (b) 1-cycle, (c) 3-cycle and (d) 7-cycle ARB processed specimens.

[DOI: 10.22068/ijmse.17.1.1]

is also observed. It should be noted that the 1-cycle ARB is only equal to the conventional rolling process (50% reduction in thickness). Our results are consistent with a previous study which has indicated that the copper component ({112}<111>) is a dominant texture in FCC metals after conventional rolling [32]. With the progress of deformation strain, the copper component ({112}<111>) disappeared in favor of the rotated cube orientation ({100}<110>) in the 3-cycle ARB processed specimen.

Fig. 5 represents the ODFs of the starting material, 1-cycle, 3-cycle, and 7-cycle ARB processed specimens. As shown in Fig. 5 (a), the starting material has a random texture with low ODF intensity. 1-cycle of the ARB causes a strong copper orientation ({112}<111>), and by increasing the number of ARB cycles a kind of texture transition appears. This means rotated cube orientation ({100}<110>) is developed as the main preferred orientation in the 3-cycle and 7-cycle ARB processed specimens as indicated in Fig. 5 (b), (c) and (d). It should be noted that the Goss component ({110}<001>) is also observed in the 7-cycle ARB processed specimen.

In previous studies [28,33], it was well established that the rotated cube ({100}<110>) is the main shear texture that can be developed during the ARB in FCC metals. Also, it has been reported that owing to great friction between the rolls and the specimen, a large value of redundant strain can be stored on top surfaces of the strips during the ARB process [28,34]. Since no lubricant was used during the processes of this research, it was expected that very large friction, present between rolls and the specimen, resulted in the formation

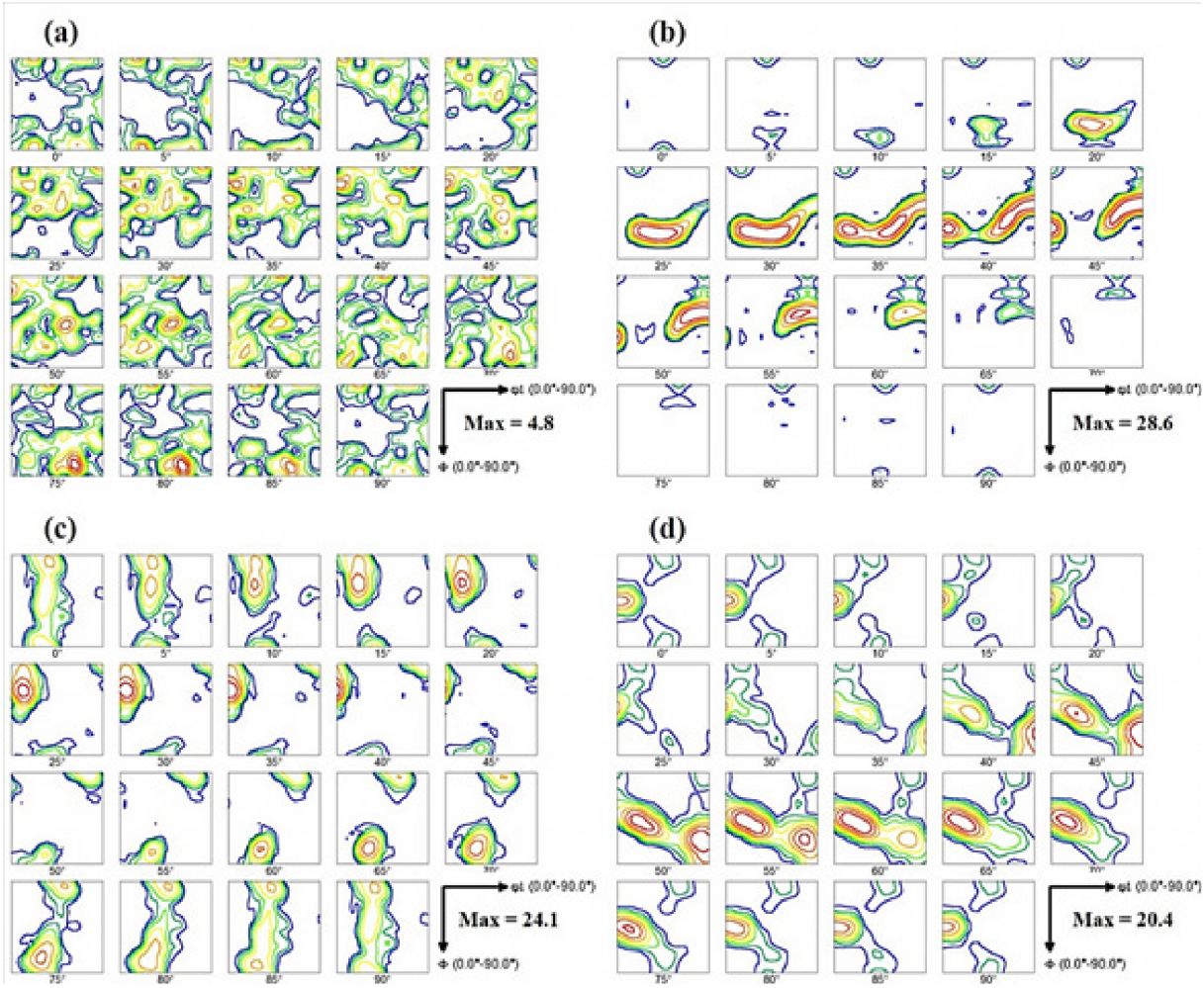

Fig. 5. ODFs of (a) the starting material, (b) 1-cycle, (c) 3-cycle and (d) 7-cycle ARB processed specimens.

[DOI: 10.22068/ijmse.17.1.1]

of a strong rotated cube ({100}<110>) texture near the surface of the sample even by 1-cycle of the ARB. This texture could then propagate inward the specimen thickness by increasing the ARB cycles. Since the strips are cut and stacked in every cycle; half of the surface that has undergone severe deformation comes into the center as shown in Fig. 1. As a result, the surfaces have shear texture propagated inward of the sample.

3.3. Mechanical Properties

Engineering stress-strain curves are presented in Fig. 6. The results indicate that the starting material exhibits yield strength of about 150 MPa along with a large elongation above 20%. As it is illustrated, both yield and tensile strengths boosted after each ARB cycle. Other researchers have also observed similar trends in the ARB processed aluminum and steel alloys [2,3,14,35]. The ARB processed specimens show high strength and low elongation, which are the typical behavior of ARB processed materials.

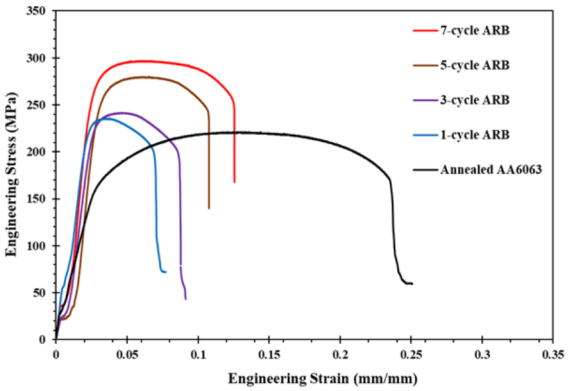

Fig. 6. The engineering stress-strain curves of annealed and ARB processed AA6063 specimens at different cycles.

The effect of the number of ARB cycle on the mechanical properties of AA6063 alloy is indicated in Fig. 7. The yield strength and tensile strength increase from 150 MPa and 190 MPa in the state of the annealed specimen to 195 MPa and 234 MPa even after one cycle of the ARB, registering 30% and 23% improvement, respectively. After 7 cycles of ARB, the yield strength and tensile strength increased up to about 258 MPa and 300 MPa, respectively. The characteristic nature of this plot shows that the ultimate tensile strength and yield strength increases by 72% and 60%, respectively after seven cycles of ARB. According to Fig. 7, total elongation for the starting material varies between 25-30% compared to 11-13% in the case of ARB processed AA6063 alloy.

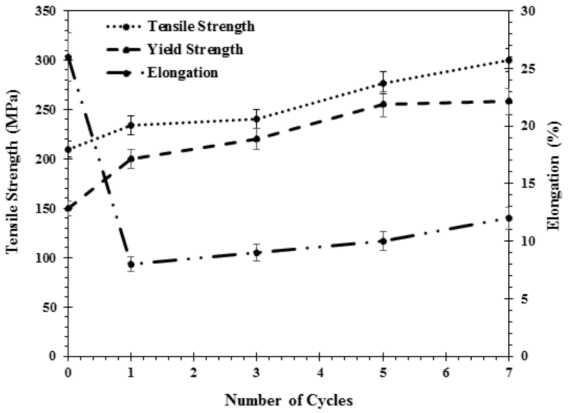

Fig. 7. Tensile strength, yield strength and elongation variations of AA6063 specimens for various ARB cycles.

It is well known that decreasing the ductility or uniform elongation after ARB processing is mainly attributed to strain hardening which causes the mobility of dislocations to decrease, and therefore, the ductility declines [3, 33-36]. The higher elongation in high-cycles ARB materials may have corresponded to more homogeneity of microstructures as described later. In high-cycle ARB processed materials, homogeneity develops more, which leads to the effective and uniform accumulation of dislocation and results in high strain hardening capability. In contrast, in low-cycle ARB materials, inhomogeneity of microstructures is considerable, which lead to inhomogeneity accumulation of dislocations. Such inhomogeneity accumulation of dislocations leads to local high-stress concentration and debonding at an early stage, which results in the appearance of low ductility. Furthermore, the unique shear texture may enhance the anisotropy of plasticity (R-value) and may help to enhance the ductility in high-cycle ARB materials.

The change in grain size obtained from EBSD data is summarized in Fig. 8 as a function of the ARB cycle. It is well clarified that when the number of ARB cycles increase the average

[DOI: 10.22068/ijmse.17.1.1]

grain size decline gradually in EBSD results. Increment of yield strength essentially depends on grain size based on the Hall-Petch relationship. Hence, it is predictable that the yield strength boosted step by step as the number of ARB cycle increases and as a result, the grain size decreases as well indicated in Fig. 7.

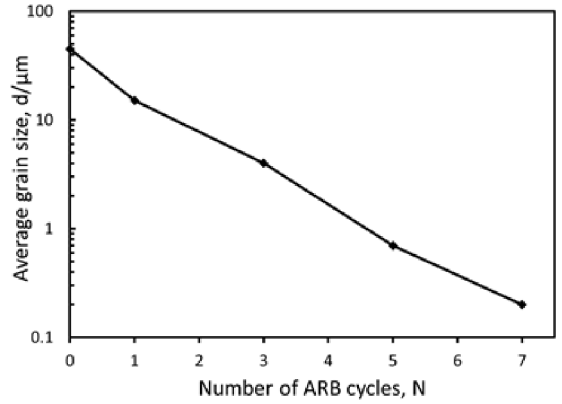

Fig. 8. Average grain size variations as a function of ARB cycles.

Figure 9 (a) shows the variations of microhardness and inhomogeneity factor for AA6063 alloy during ARB cycles. A drastic enhancement can be observed in the hardness value after the first cycle, which is almost 86% greater than that of the annealed specimen. The significant increase in microhardness after the first cycle seems to be related to the high rate of strain hardening which is due to high dislocation density. After the first cycle, microhardness rapidly increased, then the rate of this growth dwindled and finally saturated by further ARB cycles. This result is in consistent with the previous researchers' works on the accumulative roll bonding process [36,37]. Figure 8 (b) indicates that a major increase in the inhomogeneity factor occurred after the first cycle of ARB proposing a large deformation inhomogeneity for that specimen. However, as the number of ARB cycles increased, the inhomogeneity factor values reduced, which is an indication of improvement in the deformation homogeneity during later cycles.

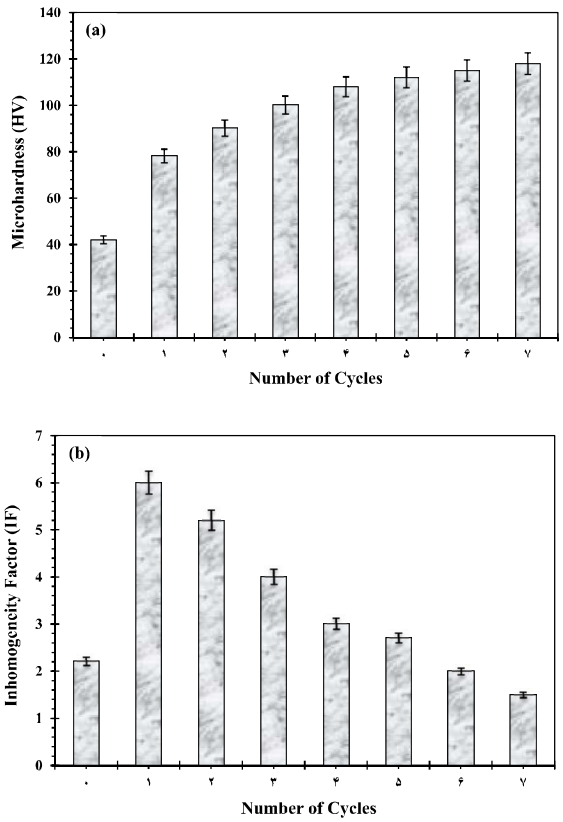

Fig. 9. The variation of (a) microhardness and (b) inhomogeneity factor as a function of ARB cycles number for AA6063 specimens.

3.4. Fractography

As seen in Fig. 10, the large size of dimples generated from the initial material suggests a highly ductile mode of fracture behavior [38]. Ductile fracture normally occurs in a transgranular manner in metals that have decent ductility and toughness [39]. By increasing the number of ARB cycles, the dimples are small and elongated, which clearly shows that the failure mode is shear ductile rupture. In fact, this mode is characterized by shallow, small, and elongated shear dimples. Also, Fig. 10 shows that the fractography results of ARB processed specimens indicate the improvement in bond strength brought forward from the previous cycles.

[DOI: 10.22068/ijmse.17.1.1]

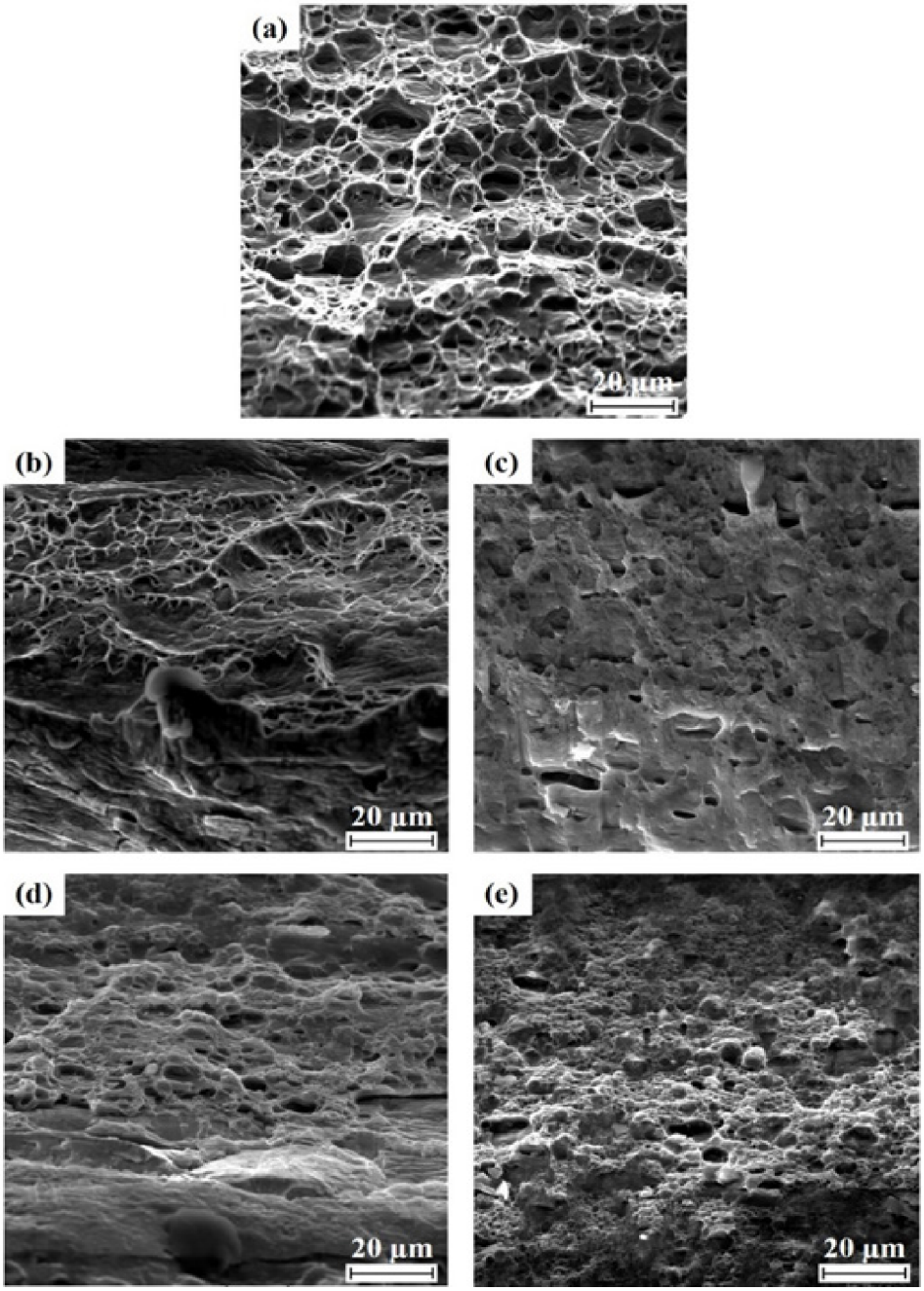

Fig. 10. Tensile fractured surfaces of (a) annealed and ARB processed AA6063 specimens after (b) 1, (c) 3, (d) 5 and (e) 7 cycles.

4. CONCLUSIONS

Texture development and mechanical properties with respect to microstructure evolution in an AA6063 alloy processed by the accumulative roll bonding process at room temperature were investigated. The conclusions drawn from the results can be summarized as follows:

1. With increasing the number of ARB cycles, the average grain size of samples decreased and finally, after 7 cycles reached 200 nm.
2. After 1 ARB cycles, the major texture components in the ARB processed AA6064 exhibits mainly deformation texture of high stacking fault FCC metals, i.e., copper ({112}<111>) and Dillamore ({4 4 11}<11 11 8>)

[DOI: 10.22068/ijmse.17.1.1]

orientations.

3. By increasing the number of ARB process cycles to 3 and 7, the texture is significantly intensified near the rotated cube orientation ({100}<110>) and Goss orientation ({110}<001>) which are known as shear textures.
4. Yield strength and tensile strength increases with increasing strain and decreasing the grain size of the ARB processed specimens.
5. The fracture surface of all specimens is characterized by the large size of dimples with large voids, as a typical ductile fracture mode.

ACKNOWLEDGMENTS

The financial support of the Center for International Scientific Studies and Collaboration (CISSC), Ministry of Science, Research and Technology (MSRT) is gratefully acknowledged.

REFERENCES

1. Jafarian, H. R. and Tarazkouhi, M. F., "Significant enhancement of tensile properties through combination of severe plastic deformation and reverse transformation in an ultrafine/nano grain lath martensitic steel", Mater. Sci. Eng. A. 2017, 686, 113–120.
2. Tirekar, S., Jafarian, H. R. and Eivani, A. R., "Towards engineering of mechanical properties through stabilization of austenite in ultrafine grained martensite–austenite dual phase steel processed by accumulative roll bonding", Mater. Sci. Eng. A. 2017, 120–126.
3. H., Jafarian, "Characteristics of nano/ultrafine-grained austenitic TRIP steel fabricated by accumulative roll bonding and subsequent annealing", Mater. Charact. 2016, 114, 88–96.
4. Valiev, R. Z., Korznikov, A. V. and Mulyukov, R. R., "Structure and properties of ultrafine-grained materials produced by severe plastic deformation", Mater. Sci. Eng. A. 1993, 168, 141–148.
5. Azushima, A., Kopp, R., Korhonen, A., Yang, D. Y., Micari, F., Lahoti, G. D., Groche, P., Yanagimoto, J., Tsuji, N. and Rosochowski, A., "Severe plastic deformation (SPD) processes for metals", CIRP Ann.-Manuf. Technol. 2008, 57, 716–735.
6. Valiev, R. Z., Islamgaliev, R. K. and Alexandrov, I. V. "Bulk nanostructured materials from severe plastic deformation", Prog. Mater. Sci. 2000, 45, 103–189.
7. Tsuji, N., Saito, Y., Lee, S. H. and Minamino, Y., "ARB (Accumulative Roll-Bonding) and other new techniques to produce bulk ultrafine grained materials", Adv. Eng. Mater. 2003, 5, 338–344.
8. Jafarian, H., Habibi-Livar, J. and Razavi, S. H., "Microstructure evolution and mechanical properties in ultrafine grained Al/TiC composite fabricated by accumulative roll bonding, Compos. Part B Eng. 2015, 77, 84–92.
9. Jafarian, H. R. and Habibi-Livar, J., "Dependency of annealing behaviour on grain size in Al–TiC composite produced by accumulative roll bonding", Bull. Mater. Sci. 2017, 40, 583–590.
10. Jahromi, K. G., Zarei-Hanzaki, A. and Golmahalleh, O., "Ultra fine ferrite formation in Si-Mn trip steels", Iran. J. Mater. Sci. Eng. 2008, 5, 1–7.
11. Jafarian, H. R., Anijdan, S. M., Eivani, A. R. and Park, N., "A comprehensive study of microstructure development and its corresponding tensile properties in nano/ultrafine-grained metastable austenitic steel during accumulative roll bonding (ARB)", Mater. Sci. Eng. A. 2017, 703, 196–204.
12. Yazdani, A., Salahinejad, E., Moradgholi, J. and Hosseini, M., "A new consideration on reinforcement distribution in the different planes of nanostructured metal matrix composite sheets prepared by accumulative roll bonding (ARB)", J. Alloys Compd. 2011, 509, 9562–9564.
13. Fujii, H., Cui, L., Tsuji, N., Maeda, M., Nakata, K. and Nogi, K., "Friction stir welding of carbon steels", Mater. Sci. Eng. A. 2006, 429, 50–57.
14. Borhani, E., Jafarian, H., Terada, D., Adachi, H. and Tsuji, N., "Microstructural Evolution during ARB Process of Al-0.2 mass% Sc Alloy Containing Al3Sc Precipitates in Starting Structures", Mater. Trans. 2012, 53, 72–80.
15. Eizadjou, M., Talachi, A. K., Manesh, H. D., Shahabi, H. and Janghorban, S., K., "Investigation of structure and mechanical properties of multi-layered Al/Cu composite produced by accumulative roll bonding (ARB) process", Compos. Sci. Technol. 2008, 68, 2003–2009.
16. Sato, Y. S., Yamanoi, H., Kokawa, H. and Furuhara, T., "Microstructural evolution of ultrahigh carbon steel during friction stir welding", Scr. Mater. 2007, 57, 557–560.
17. Alizadeh, M. and Paydar, M. H., "Fabrication of nanostructure Al/SiC P composite by accumulative roll-bonding (ARB) process", J. Alloys Compd. 2010, 492, 231–235.
18. Tsuji, N., Saito, Y., Utsunomiya, H. and Tanigawa, S., "Ultra-fine grained bulk steel produced by accumulative roll-bonding (ARB) process", Scr. Mater. 1999, 40, 795–800.

[DOI: 10.22068/ijmse.17.1.1]

19. Sugimoto, K. I., Kobayashi, M. and Hashimoto, S. I., "Ductility and strain-induced transformation in a high-strength transformation-induced plasticity-aided dual-phase steel", Metall. Trans. A. 1992, 23, 3085–3091.
20. Höppel, H. W., May, J. and Göken, M., "Enhanced strength and ductility in ultrafine-grained aluminium produced by accumulative roll bonding", Adv. Eng. Mater. 2004, 6, 781–784.
21. Kumar, S. S. and Raghu, T., "Structural and mechanical behaviour of severe plastically deformed high purity aluminium sheets processed by constrained groove pressing technique", Mater. Des. 2014, 57, 114–120.
22. Tsuji, N., Iwata, T., Sato, M., Fujimoto, S., Minamino, Y., "Aging behavior of ultrafine grained Al–2 wt% Cu alloy severely deformed by accumulative roll bonding", Sci. Technol. Adv. Mater. 2004, 5, 173.
23. Arigela, V. G., Palukuri, N. R., Singh, D., Kolli, S. K., Jayaganthan, R., Chekhonin, P., Scharnweber, J. and Skrotzki, W., "Evolution of microstructure and mechanical properties in 2014 and 6063 similar and dissimilar aluminium alloy laminates produced by accumulative roll bonding", J. Alloys Compd. 2019, 790, 917–927.
24. Hughes, D. A. and Hansen, N., "High angle boundaries formed by grain subdivision mechanisms", Acta Mater. 1997, 45, 3871–3886.
25. Hansen, N., Mehl, R. F. and Medalist, A., "New discoveries in deformed metals", Metall. Mater. Trans. A. 2001, 32, 2917–2935.
26. Hansen, N. and Jensen, D. J., "Development of microstructure in FCC metals during cold work", Philos. Trans. R. Soc. Lond. Math. Phys. Eng. Sci. 1999, 357, 1447–1469.
27. Hansen, N., "Boundary strengthening in undeformed and deformed polycrystals", Mater. Sci. Eng. A. 2005, 409, 39–45.
28. Kamikawa, N., Sakai, T. and Tsuji, N., "Effect of redundant shear strain on microstructure and texture evolution during accumulative roll-bonding in ultralow carbon IF steel", Acta Mater. 2007, 55, 5873–5888.
29. Jamaati, R., Toroghinejad, M. R., Hoseini, M. and Szpunar, J. A., "Development of texture during ARB in metal matrix composite", Mater. Sci. Technol. 2012, 28, 406–410.
30. Borhani, E., Jafarian, H., Shibata, A. and Tsuji, N., "Texture Evolution in Al–0.2 mass% Sc Alloy during ARB Process and Subsequent Annealing", Mater. Trans. 2012, 53, 1863–1869.
31. Jafarian, H. and Eivani, A., "Texture development and microstructure evolution in metastable austenitic steel processed by accumulative roll bonding and subsequent annealing", J. Mater. Sci. 2014, 49, 6570–6578.
32. Jamaati, R. and Toroghinejad, M. R., "Effect of stacking fault energy on deformation texture development of nanostructured materials produced by the ARB process", Mater. Sci. Eng. A. 2014, 598, 263–276.
33. Jamaati, R., Toroghinejad, M. R., Mohtadi-Bonab, M. A., Edris, H., Szpunar, J. A. and Salmani, M. R., "The effect of SiC nanoparticles on deformation texture of ARB-processed steel-based nanocomposite", Mater. Charact. 2014, 93, 150–162.
34. Jamaati, R. and Toroghinejad, M. R., "Effect of alloy composition, stacking fault energy, second phase particles, initial thickness, and measurement position on deformation texture development of nanostructured FCC materials fabricated via accumulative roll bonding process", Mater. Sci. Eng. A. 2014, 598, 77–97.
35. Samaee, M., Najafi, S., Eivani, A. R., Jafarian, H. R. and Zhou,J., "Simultaneous improvements of the strength and ductility of fine-grained AA6063 alloy with increasing number of ECAP passes", Mater. Sci. Eng. A. 2016, 669, 350–357.
36. Toroghinejad, M. R., Ashrafizadeh, F. and Jamaati, R., "On the use of accumulative roll bonding process to develop nanostructured aluminum alloy 5083", Mater. Sci. Eng. A. 2013, 561, 145–151.
37. Jafarian, H. R., Borhani, E., Shibata, A., Terada, D. and Tsuji, N., "Martensite/austenite interfaces in ultrafine grained Fe–Ni–C alloy", J. Mater. Sci. 2011, 46, 4216–4220.
38. Cavaliere, P., "Fatigue properties and crack behavior of ultra-fine and nanocrystalline pure metals", Int. J. Fatigue. 2009, 31, 1476–1489.
39. Pardoen, T., Dumont, D., Deschamps, A. and Brechet, Y., "Grain boundary versus transgranular ductile failure", J. Mech. Phys. Solids. 2003, 51, 637–665.

[DOI: 10.22068/ijmse.17.1.1]